Editors' Suggestion

Coulomb Drag between a Carbon Nanotube and Monolayer Graphene

Laurel Anderson,[1] Austin Cheng,[2] Takashi Taniguchi,[3] Kenji Watanabe,[4] and Philip Kim[1,2,*]
[1]Department of Physics, Harvard University, Cambridge, Massachusetts 02138, USA
[2]Department of Applied Physics, Harvard University, Cambridge, Massachusetts 02138, USA
[3]International Center for Materials Nanoarchitectonics, National Institute for Materials Science, Tsukuba 305-0044, Japan
[4]Research Center for Functional Materials, National Institute for Materials Science, Tsukuba 305-0044, Japan

(Received 15 June 2021; revised 15 September 2021; accepted 11 November 2021; published 13 December 2021)

We have measured Coulomb drag between an individual single-walled carbon nanotube (SWNT) as a one-dimensional (1D) conductor and the two-dimensional (2D) conductor monolayer graphene, separated by a few-atom-thick boron nitride layer. The graphene carrier density is tuned across the charge neutrality point (CNP) by a gate, while the SWNT remains degenerate. At high temperatures, the drag resistance changes sign across the CNP, as expected for momentum transfer from drive to drag layer, and exhibits layer exchange Onsager reciprocity. We find that layer reciprocity is broken near the graphene CNP at low temperatures due to nonlinear drag response associated with temperature dependent drag and thermoelectric effects. The drag resistance shows power-law dependences on temperature and carrier density characteristic of 1D Fermi liquid-2D Dirac fluid drag. The 2D drag signal at high temperatures decays with distance from the 1D source slower than expected for a diffusive current distribution, suggesting additional interaction effects in the graphene in the hydrodynamic transport regime.

DOI: 10.1103/PhysRevLett.127.257701

Coulomb interactions generate a plethora of novel emergent phenomena in condensed-matter systems, particularly when electronic confinement to fewer than three spatial dimensions increases the relative strength of potential to kinetic energy [1]. One experimental tool for studying interaction-driven effects in low-dimensional systems is Coulomb drag [2–5]. When a current is driven in a conductor that is near but electrically isolated from another, Coulomb interactions between the charge carriers in the two conductors generate a voltage drop in the passive conductor. The drag resistance is thus a direct probe of interlayer charge carrier interaction. Most of the past theoretical and experimental efforts have focused on drag between two-dimensional (2D) conductors, such as electrons confined in semiconductor heterointerfaces [3,4] and graphene [5–7], revealing several new emergent phenomena including exciton condensation under strong magnetic fields [5]. Drag experiments have also been performed between one-dimensional (1D) conductors [8–10], showing signatures of Wigner crystal and Luttinger liquid behavior.

Coulomb drag experiments between mixed-dimensional systems, e.g., 1D-2D conductors, have also been conceived [11,12] to investigate the effects of dimensionality on electron-electron interactions. Such a system was recently probed experimentally [13] using an InAs nanowire as 1D conductor and graphene as 2D conducting layer. This recent 1D-2D drag experiment shows an anomalous temperature and density dependent drag response that might be related to energy drag [14–16] due to the large mismatch in thermal conductivities between InAs and graphene. However, the breakdown of layer (Onsager) reciprocity and subsequent thermopower measurements in these devices [17] suggest local heating-induced thermoelectric effects may also play a substantial role in the reported drag results.

In this Letter, we report Coulomb drag in a new 1D-2D conducting system, a metallic single-walled carbon nanotube (SWNT) and monolayer graphene separated by an atomically thin (2–4 nm) insulating barrier of hexagonal boron nitride (hBN). Since SWNTs and graphene have similar linear dispersion relations with comparable Fermi energies and work functions [18,19], the interaction-driven momentum and energy transfer between carriers in separate layers are enhanced, amplifying the drag signal. Because of the small (∼2 nm) diameter of the SWNT, driving current in the nanotube provides an extremely localized 1D drag source in the graphene channel. We measure density, temperature, and distance dependence of the drag effect to probe the carrier interactions between these 1D and 2D conductors. This work is an early step toward experimentally addressing the specific impact of increased confinement on interaction effects, and may also be a new test system for hydrodynamics in graphene.

A scanning electron microscope image of an example SWNT-graphene drag device is shown in Fig. 1(a). Details of the fabrication are given in the Supplemental Material [20]. In brief, monolayer graphene is encapsulated in hBN and then transferred on top of a metallic SWNT. The hBN flake separating the SWNT and graphene is 2–4 nm thick, so that the two conductors are sufficiently close together for

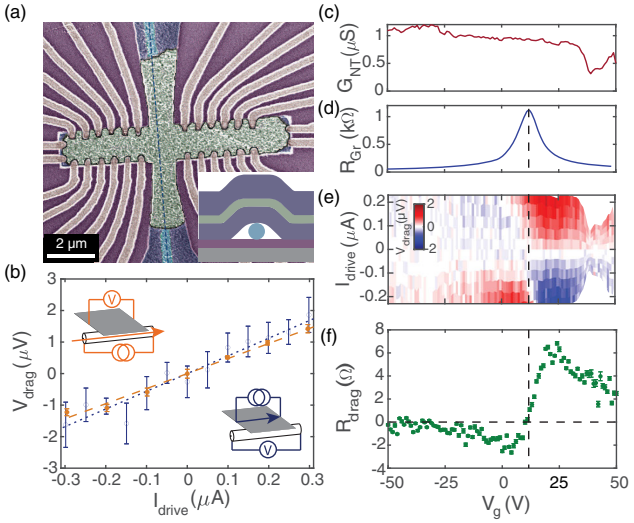

FIG. 1. (a) False color scanning electron microscope image of a typical SWNT-graphene drag device. Graphene (green) is encapsulated in hBN (dark blue) and transferred on top of a metallic SWNT (dashed line in center of blue charged region). Electrical contacts (gold) are made to the graphene and SWNT. Inset: cross-section schematic of the device. (b) V_{drag} versus I_{drive} for reciprocal layer configurations: nanotube-drive, graphene-drag (orange, filled symbols) and graphene-drive, nanotube-drag (blue, open symbols). Data were taken at $T = 300$ K and $V_g = 21$ V, with averaging gate voltage window $\Delta V = \pm 1$ V to enhance the signal-to-noise ratio. Dashed curves are lines of best fit. Additional details can be found in the Supplemental Material [20]. (c) SWNT conductance as a function of gate voltage. The dip is a local conductance minimum, not the charge neutrality point (see Supplemental Material [20] for discussion). (d) Graphene resistance as a function of gate voltage. (e) V_{drag} in graphene versus SWNT I_{drive} and V_g. (f) R_{drag} versus V_g. Dashed line marks zero drag signal.

interlayer Coulomb interactions, but they remain electrically isolated, without a significant tunneling current. The graphene and SWNT have individual electrical contacts, allowing them to be characterized separately. We can use graphene or nanotube as either drive or drag layer. While we focus on one SWNT in the following discussion, several SWNT-graphene devices were measured, and similar results were obtained (see Supplemental Material [20]).

Measurements of the drag resistance were performed by applying dc current I_{drive} through the drive layer (SWNT or graphene) while the voltage V_{drag} was measured in the drag layer (graphene or SWNT). Example data for both configurations are presented in Fig. 1(b). When using the SWNT as drive layer, V_{drag} in graphene is measured with the voltage probes nearest the SWNT, at a distance $x = 800$ nm away (closed circles). At temperature $T = 300$ K, there is a linear relationship between I_{drive} and V_{drag}, whether the SWNT or the Gr is the drive layer. Using the graphene as the drive layer and measuring V_{drag} across the SWNT (open circles) results in a noisier signal than the reciprocal drag scheme, due to the higher resistance of the SWNTs (see Supplemental Material [20] for discussion). Even so, both biasing configurations yield the same current-voltage relationship. This Onsager reciprocity when drive and drag layers are exchanged demonstrates that the system is in the linear response regime, allowing the extraction of the drag resistance from the slope: $R_{drag} = \Delta V_{drag}/\Delta I_{drive}$.

In our devices, the SWNTs are beneath the graphene [Fig. 1(a) inset], enabling the carrier densities in both SWNT and graphene to be tuned by a voltage V_g applied to a back gate. Figures 1(c) and 1(d) show the conductance G_{NT} of SWNT and resistance R_{Gr} of graphene, respectively, as a function of V_g measured at $T = 300$ K. The gradual decrease of G_{NT} as V_g increases indicates the SWNT is hole doped. In the graphene, R_{Gr} exhibits a peak corresponding to the charge neutrality point (CNP) around gate voltage $V_0 = 13$ V. We also measure the drag response as a function of V_g, as shown in Fig. 1(e). We extract R_{drag} in the linear response regime in as a function of V_g, as described above. For $V_g < V_0$, V_{drag} and I_{drive} have opposite sign, while for $V_g > V_0$, they have the same sign. As shown in Fig. 1(f), R_{drag} thus changes sign at $V_g = V_0$ where the dominant carrier type in graphene switches from electrons to holes. This behavior is qualitatively similar to previous measurements of momentum-transfer Coulomb drag in double-layer graphene systems [6,7]. The higher magnitude of e-h compared to h-h drag can be attributed to the higher density of holes in the SWNT at more negative gate voltages. Because of heavy SWNT doping, the k_Fs of the SWNT and graphene do not overlap within our experimental gate window (further discussion in Supplemental Material [20]), preventing us from investigating the double neutrality point, where the chiral nature of the 1D-2D Dirac system can be explored [43].

As T decreases, the relationship between drive current and drag voltage becomes increasingly nonlinear [Fig. 2(a)]. To quantitatively address this change, we fit V_{drag} with a 3rd-order polynomial in I_{drive}: $V_{drag} = I_{drive}R_{drag} + \gamma I_{drive}^2 + \eta I_{drive}^3$, where γ and η are fitting coefficients. The nonlinear effect sensitively varies with V_g; Figs. 2(b)–2(c) show the V_g dependence of γ and η at several fixed temperatures. We find that $\gamma > 0$ and $\eta < 0$ for all gate voltage ranges we probe, and both quantities have larger magnitude nearer the CNP of graphene ($V_g \approx V_0$) and at lower temperatures. This increasingly nonlinear effect also breaks Onsager layer reciprocity at low temperatures. As shown in Figs. 2(d) and 2(e), the drag resistance from SWNT-drive and graphene-drive configurations show progressively worse correspondence at lower temperatures, as the nonlinear part of the relation between I_{drive} and V_{drag} becomes appreciable.

Higher-order dependence of V_{drag} on I_{drive} is best explained by development of a temperature gradient in

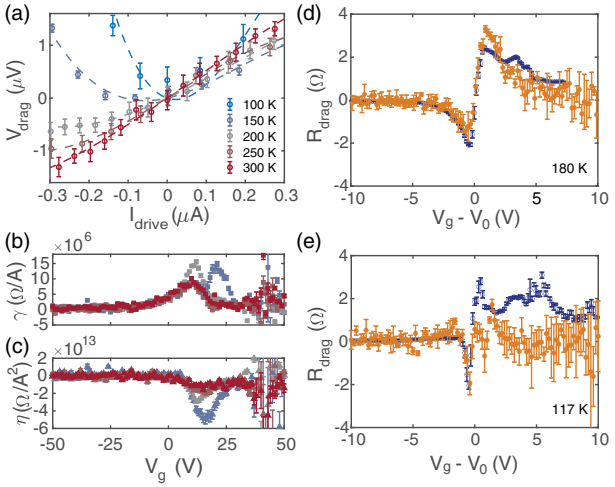

FIG. 2. (a) V_{drag} versus I_{drive} at $V_g = 22$ V for varying temperatures. Dashed lines are 3rd order polynomial fits. (b) 2nd order coefficient versus V_g. (c) 3rd order coefficient versus V_g. Regions of noisy data in (b) and (c) are due to SWNT local conductance dip limiting I_{drive}. (d) R_{drag} from linear fit versus V_g (subtracting the graphene CNP voltage) for reciprocal configurations at $T = 180$ K [same colors and symbols as Fig. 1(b)]. (e) Same measurement at $T = 117$ K.

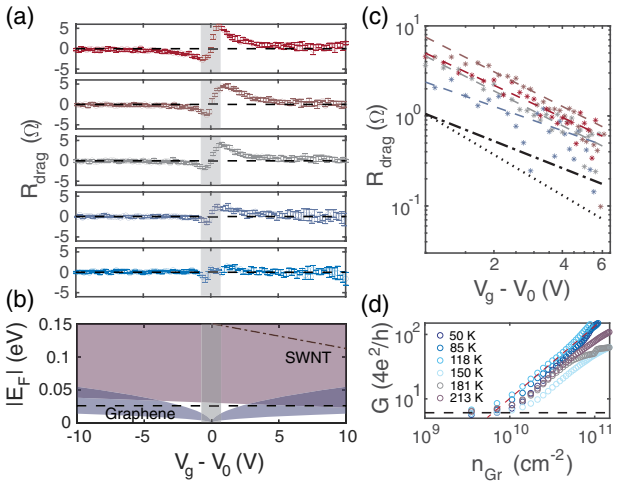

FIG. 3. (a) Drag resistance as a function of V_g at various temperatures: 265 (top), 235, 200, 160, and 130 K (bottom). Disorder-dominated range is indicated by gray shading. (b) Estimated range of Fermi energies for SWNT (purple) and graphene (blue) in a range of V_g near the graphene CNP. Dot-dashed line is approximate center of SWNT E_F range. See Supplemental Material [20] for details of calculation. (c) Log-log plot of R_{drag} versus $V_g - V_0$ at selected temperatures, with $R_{\mathrm{drag}} \propto (V_g - V_0)^{-1}$ (dot-dashed), and $R_{\mathrm{drag}} \propto (V_g - V_0)^{-1.5}$ (dotted) for comparison. (d) Graphene conductance versus charge carrier density for temperatures in (a). The residual carrier density δn is estimated by the intersection of the line at minimum conductivity (black) and a linear fit to log(G) away from charge neutrality (dark red dashed line shows example fit for $T = 118$ K).

the SWNT due to the Peltier effect or Joule heating, which can be efficiently transferred to the nearby graphene [14–16]. Such a temperature gradient in the graphene generates a thermoelectric voltage and causes a temperature-dependent change in R_{drag}. Both can give rise to nonlinear terms in V_{drag} (see Supplemental Material [20] for further analysis).

To avoid the nonlinear drag phenomena discussed above, we focus on linear drag resistance measured at small drive current at relatively high temperature ($T > 100$ K). Figure 3(a) shows R_{drag} as a function of gate voltage V_g, referenced to the CNP of graphene V_0, at different fixed temperatures in this regime. In general, R_{drag} changes sign at the graphene CNP, and that $|R_{\mathrm{drag}}|$ grows linearly, peaks, then rapidly decreases as the graphene carrier density, $n_{\mathrm{Gr}} \propto V_g - V_0$, increases. Figure 3(b) shows that $R_{\mathrm{drag}} \sim (V_g - V_0)^{-\beta}$, where $1 < \beta < 2$ at different temperatures. This behavior resembles 2D-2D graphene drag, where $1 < \beta < 2$ has also been observed [6,7].

To determine the carrier densities (and thus Fermi energies) of each conductor as a function of V_g, we employ a finite element analysis of the graphene channel and SWNT together with the hBN separation layers and silicon back gate [Fig. 1(a), inset]. Since the SWNT locally screens the graphene channel from the back gate, the local carrier density in graphene is reduced in the graphene channel directly above the SWNT and maximized away from the SWNT. To estimate the carrier density (and thus chemical potential) of the SWNT, we also need to consider device geometry and quantum capacitance (detailed discussion in Ref. [20]). Figure 3(b) summarizes the estimated upper and lower bounds of the Fermi energies of graphene E_F^{Gr} and SWNT E_F^{NT}. While the SWNT remains a heavily p-doped degenerate 1D conductor in the experimental gate voltage range, our analysis suggests that E_F^{Gr} is comparable to or even smaller than $k_B T$ in the temperature range $T > 100$ K, where k_B is the Boltzmann constant, for all V_g where the drag signal is measurable.

Near the CNP of the graphene channel, disorder becomes more relevant, creating charge puddles [44]. The n_{Gr}-dependent conductance of the graphene channel is accordingly expected to saturate at low temperatures for $|n_{\mathrm{Gr}}| < \delta n$, where δn is the residual density due to charge puddles, which can be estimated from the temperature-dependent conductance G of the graphene [45]. Figure 3(d) shows $G(n_{\mathrm{Gr}})$ measured in the graphene channel of our device for $T \lesssim 150$ K. From the saturation of $G(n_{\mathrm{Gr}})$ near the CNP, we estimate $\delta n \approx 1.1 \times 10^{10}$ cm^{-2}. For $|n_{\mathrm{Gr}}| < \delta n$, the electron and hole contributions of Coulomb drag cancel, resulting in linearly vanishing R_{drag} with n_{Gr} as observed in the experiment [shaded region in Fig. 3(a)]. We also estimate the puddle energy scale $k_B T_d = \hbar v_F \sqrt{\pi \delta n}$, where $\hbar$ and $v_F = 10^6$ m/s are the reduced Plank constant and Fermi velocity of graphene,

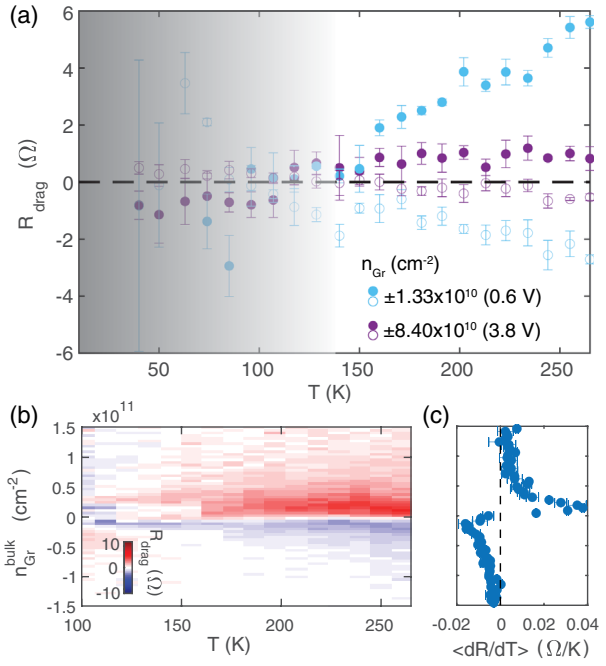

FIG. 4. (a) Drag resistance as a function of temperature for various graphene charge carrier densities (stated value is the upper bound). For $T < 140$ K (the shaded region in the graph), nonlinear effects increasingly dominate the signal. (b) Drag resistance versus temperature and graphene carrier density. (c) Average (dR_{drag}/dT) for $T > T_d$ versus temperature at a range of graphene carrier densities.

respectively. From δn experimentally obtained above, we find the disorder temperature scale $T_d \approx 140$ K, which separates the low temperature regime where disorder effects are dominant and the high temperature regime where thermal broadening is appreciable.

We find the drag near the graphene CNP depends sensitively on temperature. Figure 4(a) shows T-dependent R_{drag} at fixed density (reported as $n_{\mathrm{Gr}}^{\mathrm{bulk}}$, the upper bound of the estimated graphene carrier density). For $n_{\mathrm{Gr}}^{\mathrm{bulk}} = \pm 1.3 \times 10^{10}$ cm^{-2}, close to the peak value of $|R_{\mathrm{drag}}(n_{\mathrm{Gr}}^{\mathrm{bulk}})|$, R_{drag} increases linearly in $T - T_d$ in the high temperature regime ($T > T_d$). In the low temperature regime ($T < T_d$), however, the linear response R_{drag} is difficult to determine, due to the nonlinear drag effects and broken Onsager reciprocity discussed above. At larger density (e.g., $n_{\mathrm{Gr}}^{\mathrm{bulk}} = \pm 8.4 \times 10^{10}$ cm^{-2}, far from the CNP), we observe a similar trend, although $|R_{\mathrm{drag}}|$ is reduced. A broader range of the density and temperature-dependent $R_{\mathrm{drag}}(n_{\mathrm{Gr}}^{\mathrm{bulk}}, T)$ is shown in Fig. 4(b), where the magnitude of the drag resistance appears to increase approximately linearly at all densities. For $T > T_d$, the density dependence of (dR_{drag}/dT) behaves similarly to $R_{\mathrm{drag}}(n_{\mathrm{Gr}}^{\mathrm{bulk}})$ [Fig. 4(c)].

The temperature-dependent drag behavior discussed above is distinctly different from 2D-2D drag in graphene, where a crossover between $R_{\mathrm{drag}}(T) \sim$ constant and $R_{\mathrm{drag}}(T) \sim T^{-2}$ is expected [46] in the parameter range of our experimental regime, $E_F^{\mathrm{Gr}} \lesssim k_B T \sim E_F^{\mathrm{NT}}$. For 1D-2D drag between SWNT and graphene, Badalyan and Jauho calculated the Coulomb drag effect in the Fermi liquid regime of both conductors ($k_B T \ll E_F^{\mathrm{NT}}$, E_F^{Gr}) [47], predicting $R_{\mathrm{drag}}(T) \sim T^{\alpha}$, where $\alpha \approx 3.7$ at low temperatures. A more general theory of 1D-2D drag [12] predicts a transition to $1 < \alpha < 2$ at higher temperatures ($T > T_d$). While a more extensive model extending to the non-degenerate Dirac fluid limit in the presence of disorder is required for further quantitative comparison, our experiments show qualitatively similar behavior in the high temperature limit.

Finally, we studied the relationship between the drag signal strength and the distance of the graphene voltage probes from the SWNT. Previous experiments have demonstrated signatures of hydrodynamic electron flow from current injection into a rectangular graphene channel [48–50], with discernable effects even at room temperature [49,50]. Viscosity of the electron fluid causes the injected current to draw neighboring regions along with it, resulting in a negative potential near the injection contacts and creating current whirlpools in certain confined geometries [48,49,51,52]. Our SWNT-graphene Coulomb drag device geometry provides a unique experimental probe of hydrodynamic flow of graphene charge carriers, as the current flowing in the SWNT generates a direct dragging force on the graphene carriers without injecting current in graphene. This approach should have the benefit of eliminating diffusive spray from the contacts that could mask hydrodynamic transport signatures.

Figure 5(a) shows R_{drag} measured at pairs of voltage probes in the graphene channel laterally displaced by distance x away from the SWNT. R_{drag} decreases as x increases, becoming almost unmeasurable for $x > 2$ μm. In Ohmic transport, such a diminishing drag signal can be understood with a diffusive model, where the escaping

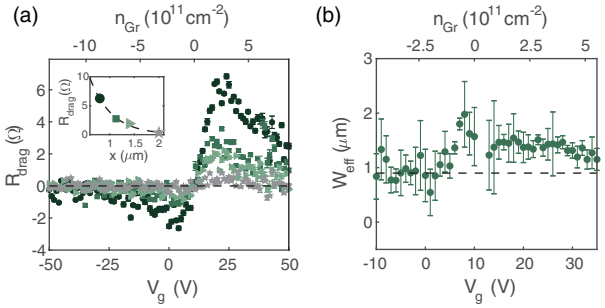

FIG. 5. (a) R_{drag} versus V_g at $T = 300$ K for pairs of voltage probes at increasing distance x from the SWNT: 800 nm (circles), 1.2 μm (squares), 1.4 μm (triangles), and 2 μm (stars). Inset: R_{drag} at $V_g = 24$ V for increasing distances. Dashed curve is an exponential fit (see main text). (b) Effective channel width W_{eff} versus V_g, extracted from fit for R_{drag} at $T = 300$ K. Dashed line marks actual device width ($W = 1$ μm).

current density in the graphene just above the SWNT is expected to decay as $J_{esc}(x) \sim e^{-\pi x/W}$, where W is the channel width [53]. In the diffusive transport regime, we therefore expect driving current in the SWNT to cause a drag voltage in the probes at distance x away following $R_{drag}(x) \sim e^{-\pi x/W}$. The inset of Fig. 5(a) shows that the measured $R_{drag}(x)$ follows such an exponential decay. We obtain the effective channel width W_{eff} by fitting this functional dependence. Figure 5(b) shows W_{eff} as a function of V_g. Interestingly, we find W_{eff} is larger than the physical channel width $W = 1$ μm in our device when the graphene is in the Dirac fluid regime, enhanced by about a factor of 2 at the CNP. Based on previous observations that the electron fluid of graphene is highly viscous in this temperature range near the CNP [48,54], the increase in W_{eff} may hint at a hydrodynamic contribution to the transport behavior.

In summary, we present an experimental study of mixed-dimensional Coulomb drag between a SWNT and graphene. Our drag measurements in a SWNT-graphene heterostructure are qualitatively consistent with momentum transfer between the drive and drag layers, although we also observe an onset of nonlinearity due to local energy transfer combined with temperature dependent drag effects at lower temperatures. Within the linear response regime, the dependences on temperature, carrier density, and distance have subtleties that suggest an interplay of different mechanisms at work in this novel hybrid system. Further measurements with higher spatial resolution, such as current imaging [50,55], would be necessary to gain a deeper understanding of the current flow patterns, and samples with less disorder should amplify hydrodynamic transport signatures in the graphene [51].

We acknowledge Leonid Levitov, Patrick Ledwith, and Artem Talanov for useful discussions. Sample preparation and device fabrication was supported by ONR MURI (N00014-16-1-2921). P. K. and A. C. acknowledge support from the ARO (W911NF-17-1-0574) for a part of measurement and analysis. L. E. A. acknowledges support from the ARO through the NDSEG Fellowship Program. K. W. and T. T. acknowledge support from the Elemental Strategy Initiative conducted by the MEXT, Japan (Grant No. JPMXP0112101001) and JSPS KAKENHI (Grants No. 19H05790 and No. JP20H00354). This work was performed, in part, at the Center for Nanoscale Systems (CNS), a member of the National Nanotechnology Infrastructure Network, which is supported by the NSF under Grant No. ECS-0335765. CNS is part of Harvard University.

*Corresponding author.
pkim@physics.harvard.edu

[1] A. Lucas and K. C. Fong, J. Phys. Condens. Matter **30**, 053001 (2018).
[2] B. N. Narozhny and A. Levchenko, Rev. Mod. Phys. **88**, 025003 (2016).
[3] T. J. Gramila, J. P. Eisenstein, A. H. MacDonald, L. N. Pfeiffer, and K. W. West, Phys. Rev. Lett. **66**, 1216 (1991).
[4] N. P. R. Hill, J. T. Nicholls, E. H. Linfield, M. Pepper, D. A. Ritchie, A. R. Hamilton, and G. A. C. Jones, J. Phys. Condens. Matter **8**, L557 (1996).
[5] X. Liu, L. Wang, K. C. Fong, Y. Gao, P. Maher, K. Watanabe, T. Taniguchi, J. Hone, C. Dean, and P. Kim, Phys. Rev. Lett. **119**, 056802 (2017).
[6] S. Kim, I. Jo, J. Nah, Z. Yao, S. K. Banerjee, and E. Tutuc, Phys. Rev. B **83**, 161401(R) (2011).
[7] R. V. Gorbachev, A. K. Geim, M. I. Katsnelson, K. S. Novoselov, T. Tudorovskiy, I. V. Grigorieva, A. H. MacDonald, S. V. Morozov, K. Watanabe, T. Taniguchi, and L. A. Ponomarenko, Nat. Phys. **8**, 896 (2012).
[8] M. Yamamoto, M. Stopa, Y. Tokura, Y. Hirayama, and S. Tarucha, Science **313**, 204 (2006).
[9] D. Laroche, G. Gervais, M. P. Lilly, and J. L. Reno, Nat. Nanotechnol. **6**, 793 (2011).
[10] D. Laroche, G. Gervais, M. P. Lilly, and J. L. Reno, Science **343**, 631 (2014).
[11] Y. M. Sirenko and P. Vasilopoulos, Phys. Rev. B **46**, 1611 (1992).
[12] S. K. Lyo, Phys. Rev. B **68**, 045310 (2003).
[13] R. Mitra, M. R. Sahu, K. Watanabe, T. Taniguchi, H. Shtrikman, A. K. Sood, and A. Das, Phys. Rev. Lett. **124**, 116803 (2020).
[14] J. C. W. Song and L. S. Levitov, Phys. Rev. Lett. **109**, 236602 (2012).
[15] J. C. W. Song, D. A. Abanin, and L. S. Levitov, Nano Lett. **13**, 3631 (2013).
[16] J. C. W. Song and L. S. Levitov, Phys. Rev. Lett. **111**, 126601 (2013).
[17] R. Mitra, M. R. Sahu, A. Sood, T. Taniguchi, K. Watanabe, H. Shtrikman, S. Mukerjee, A. K. Sood, and A. Das, arXiv: 2009.08882.
[18] E. A. Laird, F. Kuemmeth, G. A. Steele, K. Grove-Rasmussen, J. Nygård, K. Flensberg, and L. P. Kouwenhoven, Rev. Mod. Phys. **87**, 703 (2015).
[19] A. H. Castro Neto, F. Guinea, N. M. R. Peres, K. S. Novoselov, and A. K. Geim, Rev. Mod. Phys. **81**, 109 (2009).
[20] See Supplemental Material at http://link.aps.org/supplemental/10.1103/PhysRevLett.127.257701 for detailed fabrication and measurement methods, discussion of the effect of the graphene chemical potential on the observed drag, estimation of graphene and SWNT charge carrier densities, and additional experimental data. It also contains Refs. [21–42].
[21] A. Cheng, T. Taniguchi, K. Watanabe, P. Kim, and J.-D. Pillet, Phys. Rev. Lett. **123**, 216804 (2019).
[22] M. Y. Sfeir, T. Beetz, F. Wang, L. Huang, X. M. H. Huang, M. Huang, J. Hone, S. O'Brien, J. A. Misewich, T. F. Heinz, L. Wu, Y. Zhu, and L. E. Brus, Science **312**, 554 (2006).
[23] X. M. H. Huang, R. Caldwell, L. Huang, S. C. Jun, M. Huang, M. Y. Sfeir, S. P. O'Brien, and J. Hone, Nano Lett. **5**, 1515 (2005).
[24] Q. Cao, S.-J. Han, J. Tersoff, A. D. Franklin, Y. Zhu, Z. Zhang, G. S. Tulevski, J. Tang, and W. Haensch, Science **350**, 68 (2015).

[25] J.-W. Huang, C. Pan, S. Tran, B. Cheng, K. Watanabe, T. Taniguchi, C. N. Lau, and M. Bockrath, Nano Lett. **15**, 6836 (2015).
[26] W. Kim, A. Javey, R. Tu, J. Cao, Q. Wang, and H. Dai, Appl. Phys. Lett. **87**, 173101 (2005).
[27] G. Pitner, G. Hills, J. P. Llinas, K.-M. Persson, R. Park, J. Bokor, S. Mitra, and H.-S. P. Wong, Nano Lett. **19**, 1083 (2019).
[28] C. R. Dean, A. F. Young, I. Meric, C. Lee, L. Wang, S. Sorgenfrei, K. Watanabe, T. Taniguchi, P. Kim, K. L. Shepard, and J. Hone, Nat. Nanotechnol. **5**, 722 (2010).
[29] L. Wang, I. Meric, P. Y. Huang, Q. Gao, Y. Gao, H. Tran, T. Taniguchi, K. Watanabe, L. M. Campos, D. A. Muller, J. Guo, P. Kim, J. Hone, K. L. Shepard, and C. R. Dean, Science **342**, 614 (2013).
[30] J. I. A. Li, T. Taniguchi, K. Watanabe, J. Hone, A. Levchenko, and C. R. Dean, Phys. Rev. Lett. **117**, 046802 (2016).
[31] N. M. R. Peres, J. M. B. Lopes dos Santos, and A. H. Castro Neto, Europhys. Lett. **95**, 18001 (2011).
[32] S. Ilani, L. A. K. Donev, M. Kindermann, and P. L. McEuen, Nat. Phys. **2**, 687 (2006).
[33] H.-S. P. Wong and D. Akinwande, *Carbon Nanotube and Graphene Device Physics* (Cambridge University Press, Cambridge, England, 2010), pp. 139–148.
[34] K. K. Ng, *Complete Guide to Semiconductor Devices*, 1st ed. (McGraw-Hill, New York, NY, 1995).
[35] K. Zhang, Y. Feng, F. Wang, Z. Yang, and J. Wang, J. Mater. Chem. C **5**, 11992 (2017).
[36] A. Laturia, M. L. Van de Put, and W. G. Vandenberghe, npj 2D Mater. Appl. **2**, 6 (2018).
[37] J. H. Seol, I. Jo, A. L. Moore, L. Lindsay, Z. H. Aitken, M. T. Pettes, X. Li, Z. Yao, R. Huang, D. Broido, N. Mingo, R. S. Ruoff, and L. Shi, Science **328**, 213 (2010).
[38] D. C. Elias, R. V. Gorbachev, A. S. Mayorov, S. V. Morozov, A. A. Zhukov, P. Blake, L. A. Ponomarenko, I. V. Grigorieva, K. S. Novoselov, F. Guinea, and A. K. Geim, Nat. Phys. **7**, 701 (2011).
[39] R. Nicklow, N. Wakabayashi, and H. G. Smith, Phys. Rev. B **5**, 4951 (1972).
[40] W. Lu, D. Wang, and L. Chen, Nano Lett. **7**, 2729 (2007).
[41] B. Kozinsky and N. Marzari, Phys. Rev. Lett. **96**, 166801 (2006).
[42] S. J. Blundell and K. M. Blundell, *Concepts in Thermal Physics*, 2nd ed. (Oxford University Press, Oxford, 2009), pp. 413–415.
[43] E. H. Hwang, R. Sensarma, and S. Das Sarma, Phys. Rev. B **84**, 245441 (2011).
[44] J. Martin, N. Akerman, G. Ulbricht, T. Lohmann, J. H. Smet, K. von Klitzing, and A. Yacoby, Nat. Phys. **4**, 144 (2008).
[45] N. J. G. Couto, D. Costanzo, S. Engels, D. K. Ki, K. Watanabe, T. Taniguchi, C. Stampfer, F. Guinea, and A. F. Morpurgo, Phys. Rev. X **4**, 041019 (2014).
[46] B. N. Narozhny, M. Titov, I. V. Gornyi, and P. M. Ostrovsky, Phys. Rev. B **85**, 195421 (2012).
[47] S. M. Badalyan and A. P. Jauho, Phys. Rev. Research **2**, 013086 (2020).
[48] D. A. Bandurin, I. Torre, R. K. Kumar, M. Ben Shalom, A. Tomadin, A. Principi, G. H. Auton, E. Khestanova, K. S. Novoselov, I. V. Grigorieva, L. A. Ponomarenko, A. K. Geim, and M. Polini, Science **351**, 1055 (2016).
[49] A. I. Berdyugin, S. G. Xu, F. M. D. Pellegrino, R. Krishna Kumar, A. Principi, I. Torre, M. Ben Shalom, T. Taniguchi, K. Watanabe, I. V. Grigorieva, M. Polini, A. K. Geim, and D. A. Bandurin, Science **364**, 162 (2019).
[50] M. J. H. Ku, T. X. Zhou, Q. Li, Y. J. Shin, J. K. Shi, C. Burch, L. E. Anderson, A. T. Pierce, Y. Xie, A. Hamo, U. Vool, H. Zhang, F. Casola, T. Taniguchi, K. Watanabe, M. M. Fogler, P. Kim, A. Yacoby, and R. L. Walsworth, Nature (London) **583**, 537 (2020).
[51] L. Levitov and G. Falkovich, Nat. Phys. **12**, 672 (2016).
[52] F. M. D. Pellegrino, I. Torre, and M. Polini, Phys. Rev. B **96**, 195401 (2017).
[53] D. A. Abanin, S. V. Morozov, L. A. Ponomarenko, R. V. Gorbachev, A. S. Mayorov, M. I. Katsnelson, K. Watanabe, T. Taniguchi, K. S. Novoselov, L. S. Levitov, and A. K. Geim, Science **332**, 328 (2011).
[54] D. A. Bandurin, A. V. Shytov, L. S. Levitov, R. K. Kumar, A. I. Berdyugin, M. Ben Shalom, I. V. Grigorieva, A. K. Geim, and G. Falkovich, Nat. Commun. **9**, 4533 (2018).
[55] J. A. Sulpizio, L. Ella, A. Rozen, J. Birkbeck, D. J. Perello, D. Dutta, M. Ben-Shalom, T. Taniguchi, K. Watanabe, T. Holder, R. Queiroz, A. Principi, A. Stern, T. Scaffidi, A. K. Geim, and S. Ilani, Nature (London) **576**, 75 (2019).